nature communications

Article

https://doi.org/10.1038/s41467-024-52382-7

Zeolite-promoted platinum catalyst for efficient reduction of nitrogen oxides with hydrogen

Received: 6 February 2024

Accepted: 30 August 2024

Published online: 12 September 2024

Check for updates

Shaohua Xie[1,2,6], Liping Liu[3,6], Yuejin Li[4], Kailong Ye[1,2], Daekun Kim[2], Xing Zhang[2], Hongliang Xin[3] ✉, Lu Ma[5], Steven N. Ehrlich[5] & Fudong Liu[1,2] ✉

Internal combustion engine fueled by carbon-free hydrogen (H_2-ICE) offers a promising alternative for sustainable transportation. Herein, we report a facile and universal strategy through the physical mixing of Pt catalyst with zeolites to significantly improve the catalytic performance in the selective catalytic reduction of nitrogen oxides (NO_x) with H_2 (H_2-SCR), a process aiming at NO_x removal from H_2-ICE. Via the physical mixing of Pt/TiO_2 with Y zeolite (Pt/TiO_2 + Y), a remarkable enhancement of NO_x reduction activity and N_2 selectivity was simultaneously achieved. The incorporation of Y zeolite effectively captured the in-situ generated water, fostering a water-rich environment surrounding the Pt active sites. This environment weakened the NO adsorption while concurrently promoting the H_2 activation, leading to the strikingly elevated H_2-SCR activity and N_2 selectivity on Pt/TiO_2 + Y catalyst. This study provides a unique, easy and sustainable physical mixing approach to achieve proficient heterogeneous catalysis for environmental applications.

The transportation sector has a considerable impact on global climate change[1], being responsible for nearly 24% of the world's CO_2 emissions stemming from fossil fuel combustion[2]. Consequently, it is imperative to prioritize substantial CO_2 reduction within this sector. While electric powertrains powered by renewable energy hold promise, their environmental cost and limited energy capacity for heavy-duty vehicles pose significant challenges for widespread application[3]. There is another viable avenue lies in the adoption of internal combustion engines (ICE) operating on carbon-free hydrogen (H_2), which presents a promising alternative for sustainable transportation[3,4]. During the H_2 combustion process, nitrogen oxides (NO_x) are the primary environmental pollutants[5,6]. Selective catalytic reduction (SCR) of NO_x is one of the most efficient and widely used technologies for NO_x abatement in excess oxygen[6,7]. For H_2-ICE applications, H_2 extracted from the fuel tank can serve directly as a reducing agent for the SCR of NO_x (H_2-SCR)[8]. This approach may offer significant economic and environmental benefits. However, to make this technique viable, the key issue to be solved is the development of robust H_2-SCR catalyst systems, which can demonstrate excellent low-temperature NO_x reduction activity and N_2 selectivity simultaneously.

Supported platinum (Pt) and palladium (Pd) catalysts have been extensively investigated for H_2-SCR reaction[6,9,10]. Notably, Pt catalysts have shown great promise with their superior low-temperature (<150 °C) activity comparing to Pd catalysts[11,12], although there is urgent need for significant improvement in N_2 selectivity[13]. H_2 activation was considered as one of the most critical factors on Pt catalysts that could profoundly influence the H_2-SCR performance[14]. Improving H_2 activation and sustaining abundant *H species on Pt catalysts could positively promote the NO dissociation[15–17], which has been reported as the rate-determining step for the H_2-SCR reaction[18,19]. Additionally, this

[1]Department of Chemical and Environmental Engineering, Bourns College of Engineering, Center for Environmental Research and Technology (CE-CERT), Materials Science and Engineering (MSE) Program, University of California, Riverside, CA, USA. [2]Department of Civil, Environmental, and Construction Engineering, Catalysis Cluster for Renewable Energy and Chemical Transformations (REACT), NanoScience Technology Center (NSTC), University of Central Florida, Orlando, FL, USA. [3]Department of Chemical Engineering, Virginia Polytechnic Institute and State University, Blacksburg, VA, USA. [4]BASF Environmental Catalyst and Metal Solutions, Iselin, NJ, USA. [5]National Synchrotron Light Source II (NSLS-II), Brookhaven National Laboratory, Upton, New York, NY, USA. [6]These authors contributed equally: Shaohua Xie, Liping Liu. ✉e-mail: hxin@vt.edu; fudong.liu@ucr.edu; lfd1982@gmail.com

enhancement could also facilitate the formation of NH_x species, which, in some cases, have been found beneficial for the H_2-SCR reaction[14,20–23]. Currently, substantial efforts have been dedicated towards increasing the presence of metallic Pt species[24,25], as it plays a crucial role in H_2 activation. Studies have reported that specific additives could substantially enhance the NO_x reduction activity by reducing the Pt valence. For instance, the addition of Mo and Na to Pt/SiO_2[26] and the introduction of Ti species into Pt/MCM-41[13] resulted in the lowered Pt valence state, leading to widened temperature window for NO_x conversion. Additionally, the acidity or basicity of supports also strongly influenced the dispersion and chemical state of Pt[27,28], with acidic supports being beneficial for the formation of metallic Pt species therefore promoting the H_2-SCR performance[27,29]. Such strategies involving the chemical modification of Pt catalysts to form more metallic Pt species were mainly intent to enhance the H_2 activation. However, it was observed that the presence of metallic Pt species usually favored the NO adsorption over H_2 adsorption, inevitably resulting in a reduced *H coverage during H_2-SCR reaction[30]. Moreover, these chemical modification strategies were found to be effective only for specific Pt catalyst systems, and in most cases the enhancement was only restricted to NO_x reduction activity but not to N_2 selectivity. Therefore, there is urgent need to design a simple, effective and universal strategy to boost the H_2 activation while reducing the NO adsorption on Pt active sites, thus improving the low-temperature activity and N_2 selectivity in the H_2-SCR reaction on Pt-based catalysts accordingly.

Different from the sophisticated chemical modification strategies as previously reported, in this work, we successfully developed a simple, sustainable physical mixing strategy of oxide-supported Pt catalysts (e.g., Pt/TiO_2, Pt/Al_2O_3, or Pt/SiO_2) with various zeolites (e.g., H-Y, H-ZSM-5, H-chabazite (CHA), H-ferrierite (FER), or H-Beta) to significantly promote the H_2-SCR reaction. Using this facile approach that is easy to scale up in industry, a universal increase in both the H_2-SCR activity and N_2 selectivity was achieved. Focusing on a typical physically mixed catalyst system involving the extensively studied Pt/TiO_2[31,32] and commercial H-Y zeolite (i.e., Pt/TiO_2 + Y), in-depth mechanistic studies were performed through the combined experimental and theoretical approaches. It was clearly revealed that the introduction of Y zeolite facilitated the formation of water-enriched micro-environment on Pt/TiO_2, which played a crucial role in mitigating the over-strong adsorption of NO while promoting the H_2 activation on Pt sites. As a result, the disassociation of NO, a crucial step in the H_2-SCR reaction, was substantially promoted, leading to the drastic enhancement in the catalytic performance.

Results

Physical mixing of Pt catalysts and zeolites to promote the H_2-SCR reaction

The Pt/TiO_2 catalyst was prepared via a conventional incipient wetness impregnation (IWI) method using colloidal Pt precursor and a commercial TiO_2 support. In the H_2-SCR reaction under typical given condition, the Pt/TiO_2 catalyst showed NO_x conversion above 11% (Fig. 1a) and N_2 selectivity above 17% (Fig. 1b) below 250 °C. When physically mixing the Pt/TiO_2 catalyst with an inactive commercial H-Y zeolite (SiO_2/Al_2O_3 molar ratio = 30) (Fig. 1a, b), within the investigated temperature range, the Pt/TiO_2 + Y catalyst system showed substantially improved catalytic performance, with NO_x conversion above 59% and N_2 selectivity above 58% below 250 °C. In addition, this Pt/TiO_2 + Y catalyst showed much higher reaction rates and N_2 selectivity at 100 and 200 °C compared to most reported Pt and Pd catalysts (Supplementary Table 1). Such a broad operation temperature window (100–250 °C) and excellent catalytic performance from Pt/TiO_2 + Y system are highly desirable for the practical H_2-SCR application[33]. In the presence of both H_2 and O_2, NO can either be reduced by H_2 to form N_2/N_2O or be oxidized by O_2 to form NO_2 (Supplementary Fig. 1). Therefore, it is reasonable that the NO_x conversion and N_2 selectivity could hardly achieve 100% under the high space velocity H_2-SCR testing conditions with H_2O and CO_2 (500 ppm NO, 1% H_2, 10% O_2, 5% CO_2, and 5% H_2O; WHSV = 461,540 mL·$g_{Pt/TiO2}^{-1}$·h^{-1}). Comparing to Pt/TiO_2, the Pt/TiO_2 + Y system consistently showed higher selectivity towards NO reduction and lower selectivity towards NO oxidation during the H_2-SCR reaction (Fig. 1c), particularly at high temperatures. The results clearly demonstrated that the presence of Y significantly promoted the NO reduction by H_2 on Pt/TiO_2 + Y system.

To verify if there was synergy effect and how it worked between Pt/TiO_2 and Y components, we investigated the different physical mixing methods (Supplementary Fig. 2a) and see how the H_2-SCR performance was impacted. It was demonstrated that, in clear contrast to the similar catalytic performance (i.e., low NO_x conversion and low N_2 selectivity) obtained on Pt/TiO_2 + Y-front and Pt/TiO_2 + Y-rear

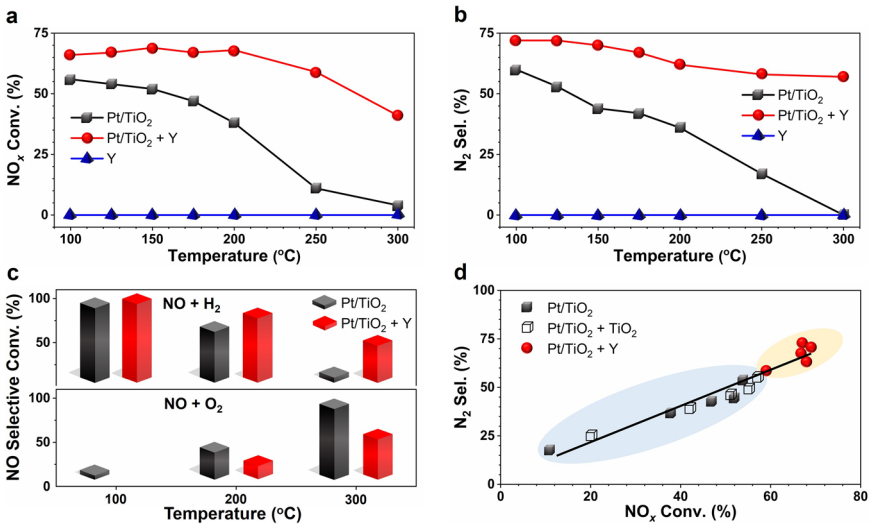

Fig. 1 | Effect of physical mixing Pt/TiO_2 with Y zeolite on the H_2-SCR performance. a NO_x conversion, and (**b**) N_2 selectivity in H_2-SCR reaction; **c** NO selective conversion (*i.e.*, NO reacting with H_2 or O_2) in H_2-SCR reaction over Pt/TiO_2 and Pt/TiO_2 + Y catalysts (see Methods section for detailed calculation); **d** Correlation between N_2 selectivity and NO_x conversion in H_2-SCR reaction over Pt/TiO_2, Pt/TiO_2 + TiO_2, and Pt/TiO_2 + Y catalysts. Reaction conditions: 26 mg of Pt/TiO_2 catalyst, or a physical mixture containing 26 mg of Pt/TiO_2 and 26 mg of Y or TiO_2; steady-state testing; 500 ppm NO, 1% H_2, 10% O_2, 5% CO_2, and 5% H_2O; weight hourly space velocity (WHSV) = 461,540 mL·$g_{Pt/TiO2}^{-1}$·h^{-1}.

systems, much more excellent H_2-SCR performance was achieved on the Pt/TiO_2 + Y system, where Pt/TiO_2 and Y powders were thoroughly physically mixed with appropriate contact (Supplementary Fig. 2b, c). To achieve even closer contact between Pt/TiO_2 and Y, we further physically mixed the Pt/TiO_2 and Y powders in the presence of water, referred as (Pt/TiO_2 + Y)_H_2O, and loaded Pt onto a pre-prepared 50% TiO_2/Y support (denoted as Pt/TiO_2/Y). It was observed that the (Pt/TiO_2 + Y)_H_2O catalyst showed slightly higher activity (Supplementary Fig. 3), and the Pt/TiO_2/Y catalyst exhibited lower activity compared to the Pt/TiO_2 + Y catalyst. However, both catalysts demonstrated lower N_2 selectivity than Pt/TiO_2 + Y catalyst. These results evidently suggest the critical role of establishing an appropriate contact between Pt/TiO_2 and Y zeolite in enhancing the overall H_2-SCR performance. As shown in Supplementary Fig. 4, the optimal content of Y in the Pt/TiO_2 + Y mixture system was determined as 50 wt%, and this formulation was simply denoted as Pt/TiO_2 + Y thereafter. To better understand this system, we also physically mixed the Pt/TiO_2 catalyst with additional TiO_2, and the Pt/Y catalyst (prepared by IWI method) with additional TiO_2 or Y, and used them as reference catalysts. As presented in Supplementary Fig. 5, the physical mixing of Pt/TiO_2 and TiO_2 showed no obvious impact on the NO_x conversion and N_2 selectivity. However, the physical mixing of Pt/Y with TiO_2 or Y resulted in considerable enhancement of the H_2-SCR performance. It was worth noting that the Pt/TiO_2 + Y formulation outperformed all other catalysts in terms of H_2-SCR activity and showed reasonable N_2 selectivity. To gain a deeper insight into the Y promotion effect, the relationship between N_2 selectivity and NO_x conversion in the H_2-SCR reaction on selected catalysts was established, as depicted in Fig. 1d. Interestingly, the N_2 selectivity versus NO_x conversion on all catalysts adhered to the same linear relationship, suggesting that the addition of Y or TiO_2 did not alter the overall H_2-SCR reaction mechanism on Pt/TiO_2 catalyst (yet the Y addition might have changed the N_2 formation pathway leading to lower N_2O production, which can be verified by the subsequent experimental results and theoretical calculations).

In addition to Y, the use of other types of zeolites for physical mixing with Pt/TiO_2 has also been explored in the H_2-SCR reaction (Supplementary Fig. 6). Remarkably, the incorporation of different zeolites such as ZSM-5, CHA, FER, and Beta also yielded substantial benefit, significantly enhancing the H_2-SCR performance. Considering both the H_2-SCR activity and N_2 selectivity in the investigated temperature range, it is evident that Y stands out as the optimal zeolite for promoting the Pt/TiO_2 catalyst. To simulate the status of catalysts for H_2-ICE exhaust purification after prolonged operation, hydrothermal aging on Pt/TiO_2 and Pt/TiO_2 + Y catalysts was conducted at 650 °C for 50 h under 10% H_2O and 10% O_2. As shown in Supplementary Fig. 7, not only before but also after the hydrothermal aging, the inclusion of Y in Pt/TiO_2 + Y system consistently exhibited remarkable enhancement on the H_2-SCR performance, with notably higher NO_x conversion and N_2 selectivity achieved than those by the zeolite-free Pt/TiO_2 catalyst. To further verify the universality of this physical mixing strategy, the H_2-SCR testing on the hydrothermally aged Pt/Al_2O_3 and Pt/SiO_2 catalysts with and without Y addition was also performed, and the results are shown in Supplementary Fig. 8. Evidently, the aged Pt/Al_2O_3 + Y and Pt/SiO_2 + Y systems demonstrated significantly enhanced activity and N_2 selectivity across the entire spectrum of reaction temperatures when contrasted with their Y-absent counterparts. It is clear that physically mixing the conventional Pt/oxide catalysts with zeolites represents a simple yet universally effective strategy for boosting the H_2-SCR performance, particularly tailored for the efficient NO_x removal from vehicle exhaust at low temperatures.

Structural characterization of Pt/TiO_2 before and after physical mixing with Y zeolite

It might be expected that the physical mixing with Y could have modified the physicochemical properties of Pt/TiO_2 leading to the distinguishable catalytic performance. We excluded this hypothesis by systematically characterizing the Pt/TiO_2 and Pt/TiO_2 + Y catalysts using multiple techniques. X-ray diffraction (XRD) (Supplementary Fig. 9) and N_2 adsorption-desorption experiments (Supplementary Fig. 10 and Supplementary Table 2) revealed that the physical mixing showed negligible impact on the crystal structure and textual properties including surface area and porosity of both Pt/TiO_2 and Y. It was observed that the Pt/TiO_2 + Y system exhibited a similar TiO_2 grain size (20.6 nm) to that of Pt/TiO_2 (20.0 nm), and its surface area (349 m^2/g) and total pore volume (0.318 cm^3/g) were approximately the mathematical average of the values for Pt/TiO_2 (81 m^2/g, 0.178 cm^3/g) and Y (709 m^2/g, 0.513 cm^3/g), respectively. Additionally, the Pt/TiO_2 + Y system demonstrated structural stability, with no apparent changes in crystal structure or textural properties after reaction at 300 °C under testing conditions with H_2O. In addition to the presence of micropores with the average diameter of 0.6 nm, Y zeolite also displayed significant mesopore defects with the average diameter of 3.8 nm that were probably formed during the dealumination process for Y zeolite production. These defects could potentially offer a substantial number of special Brønsted acidic sites (i.e., hydroxyls associated to extra-framework Al enriched on the inner pore surface), which might play a crucial role in facilitating the adsorption of H_2O molecules to occupy the mesopore structures[34]. The change of the H_2O adsorption behavior induced by Y zeolite might have altered the H_2-SCR reaction pathway on Pt/TiO_2, which will be thoroughly discussed in later sections.

As expected, the Pt particles within both Pt/TiO_2 and Pt/TiO_2 + Y catalysts showed very similar average sizes (6.0 nm vs. 6.2 nm), Pt dispersions (8.9% vs. 8.5%), CO adsorption features on Pt particle, and Pt-Pt coordination numbers (11.4 vs. 10.7), as evidenced by the characterization results of transmission electron microscopy (TEM), CO pulse titration, in situ diffuse reflectance infrared Fourier transform spectroscopy (DRIFTS) of CO adsorption, and X-ray absorption spectroscopy (XAS) (Fig. 2a, b, Supplementary Figs. 11, 12 and 13, Supplementary Table 3). Furthermore, the linear combination fitting results of X-ray absorption near-edge structure (XANES) for Pt L_3-edge demonstrated that the averaged oxidation states of Pt were 0.21 and 0.48 in Pt/TiO_2 before and after the Y addition. These values closely resembled the metallic Pt, a finding further supported by the X-ray photoelectron spectroscopy (XPS) analysis of Pt 4*d* (Supplementary Fig. 14, Supplementary Table 4). These results clearly demonstrated that the physical mixing with Y zeolite did not change the structure of Pt/TiO_2, and this conclusion was further supported by the observation of almost identical H_2 temperature-programed reduction (H_2-TPR) profiles on Pt/TiO_2 and Pt/TiO_2 + Y (Supplementary Fig. 15). Additionally, the energy dispersive spectroscopy (EDS) mapping results of Pt/TiO_2 + Y revealed that the Pt/TiO_2 components were surrounded by Y zeolite particles, without obvious direct interaction between Pt species and Y, before and after H_2-SCR reaction (Fig. 2c, Supplementary Fig. 16). Therefore, different from the chemical modifications as reported previously[24–29], the substantial enhancement in H_2-SCR performance on Pt/TiO_2 by physically mixing with Y was unequivocally attributable to the factors other than the active site modification.

Understanding on the Y promotion effect in Pt/TiO_2 + Y system

To determine the role of each reactant and the promotion effect of Y, the reaction orders of NO, H_2 and O_2 were measured for the H_2-SCR reaction. It was found that the reaction orders of NO on both Pt/TiO_2 and Pt/TiO_2 + Y were dependent on the NO partial pressure (Supplementary Fig. 17a). On Pt/TiO_2, at NO partial pressure below 25.3 Pa, the NO reaction order was determined as 0.95, while this value decreased to 0.63 at NO partial pressure above 25.3 Pa. Meanwhile, the reaction orders of H_2 and O_2 on Pt/TiO_2 were determined as 0.48 and −0.13 (Supplementary Fig. 17b, c), respectively. After physical mixing with Y, there was no evident change in the O_2 reaction order on Pt/TiO_2 + Y (only from −0.13 to −0.08). However, a notable increase in the NO

https://doi.org/10.1038/s41467-024-52382-7

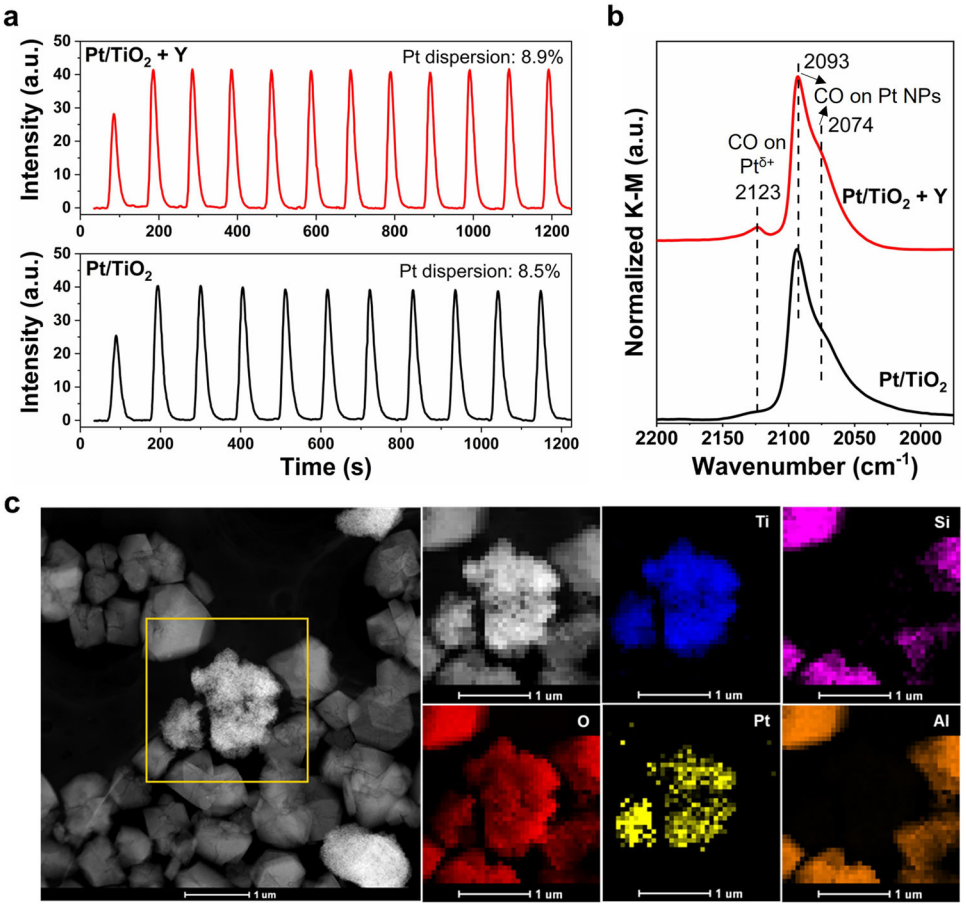

Fig. 2 | Structural characterization of Pt/TiO_2 + Y. a CO pulse titration results (with the Pt metal dispersion data inserted); **b** in situ DRIFTS of CO adsorption at 25 °C on Pt/TiO_2 and Pt/TiO_2 + Y catalysts; **c** EDS mapping images for Pt/TiO_2 + Y system.

reaction order (from 0.95 to 1.09 at lower NO partial pressure, and from 0.63 to 0.80 at higher NO partial pressure) and an obvious decrease in the H_2 reaction order (from 0.48 to 0.32) were observed on Pt/TiO_2 + Y. These results suggest that the introduction of Y probably decreased the NO adsorption, and at the same time promoted the H_2 activation because of the potential increase in H_2 coverage on catalyst surface. The enhanced H_2 activation was further supported by the experimental findings presented in Supplementary Figs. 17d and 18. The Pt/TiO_2 + Y system demonstrated superior H_2 oxidation activity compared to the Pt/TiO_2 reference, with the H_2 oxidation activity promoted further as the Y content in the Pt/TiO_2 + Y system increased (Supplementary Fig. 18). This additional increase in H_2 activation could improve the low-temperature activity and reduce the high-temperature activity, as observed on Pt/TiO_2 + Y-67% compared to that on Pt/TiO_2 + Y-50% (Supplementary Fig. 4)[14,25]. Under our testing conditions (500 ppm NO, 1% H_2, and 10% O_2), the H_2-SCR reaction rates can be expressed as: $r_{(Pt/TiO2)} = k_1 \cdot [NO]^{0.63} \cdot [H_2]^{0.48} \cdot [O_2]^{-0.13}$ and $r_{(Pt/TiO2\ +Y)} = k_2 \cdot [NO]^{0.80} \cdot [H_2]^{0.32} \cdot [O_2]^{-0.08}$, where k_1 and k_2 are constants. Notably, the NO and H_2 reaction orders on both Pt/TiO_2 (0.63 and 0.48, respectively) and Pt/TiO_2 + Y (0.80 and 0.32, respectively) are lower than 1. This suggests that the H_2-SCR reaction on both catalysts involved adsorbed NO and dissociated H* species, following the Langmuir-Hinshelwood (L-H) mechanism. Without changing the L-H mechanism, the enhanced H_2 activation could contribute to the improved H_2-SCR activity of Pt/TiO_2 + Y.

The effect of the possibly present NO_2 or NH_3 in the reaction atmosphere on H_2-SCR activity was also studied. In separate NO oxidation testing, the Pt/TiO_2 + Y system displayed noticeably lower NO oxidation activity comparing to Pt/TiO_2 (Supplementary Fig. 19a), and the presence of NO_2 in the H_2-SCR reaction atmosphere drastically decreased the low-temperature NO_x conversion on both Pt/TiO_2 and Pt/TiO_2 + Y (Supplementary Fig. 19b). Therefore, the presence of any NO_2, generated during H_2-SCR, was not responsible for the enhanced H_2-SCR activity on Pt/TiO_2 + Y. In addition, the potential promotional effect of NH_3 (possibly formed in situ through the reduction of NO_x by H_2) on H_2-SCR activity was ruled out on both Pt/TiO_2 and Pt/TiO_2 + Y. This was evident from the decrease in the H_2-SCR activity observed upon the introduction of NH_3 into the reaction stream at different temperatures (Supplementary Fig. 20).

To understand the impact of Y addition on NO adsorption behavior, the in situ DRIFTS of NO desorption at different temperatures and NO-temperature programmed desorption (NO-TPD) were conducted on Pt/TiO_2 and Pt/TiO_2 + Y catalysts. As shown in Fig. 3a, the NO adsorption on Pt/TiO_2 at 100 °C showed three distinctive bands, corresponding to bridging nitrates (1618 cm^{-1}), bidentate nitrates (1586 cm^{-1}), and monodentate nitrates (1521 cm^{-1})[35,36]. In clear contrast, the NO adsorption on Pt/TiO_2 + Y exhibited a significantly lower intensity, with the disappearance of monodentate nitrates (Fig. 3b). As the temperature elevated, the nitrate species on both Pt/TiO_2 and Pt/TiO_2 + Y catalysts decreased in intensity, following the sequence of monodentate nitrates > bidentate nitrates > bridging nitrates (Fig. 3a and b). An initial upswing in the bridging nitrates on Pt/TiO_2 was noted, attributed to the intrinsic transformation within the different types of nitrate species[37]. To assess the NO adsorption affinity, the normalized intensities of bidentate nitrates were presented at different temperatures (Fig. 3c). A much more rapid nitrate desorption from Pt/TiO_2 + Y was observed comparing to that from Pt/TiO_2. Such results unequivocally demonstrated the substantial inhibitory effect of Y zeolite on

https://doi.org/10.1038/s41467-024-52382-7

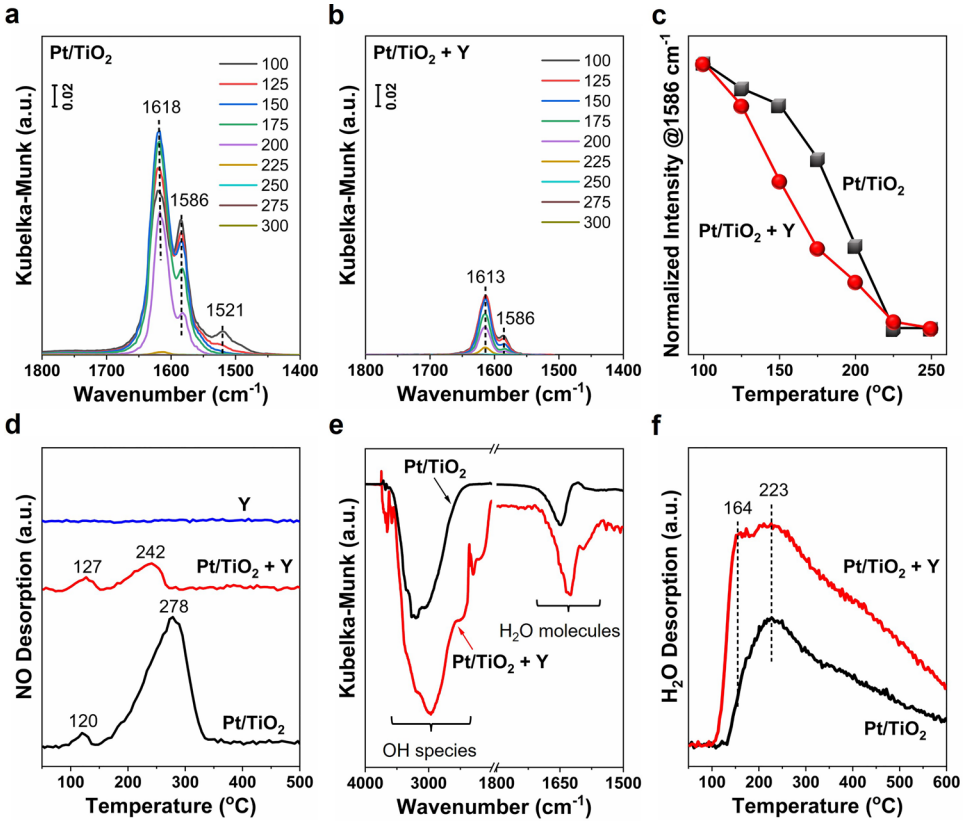

Fig. 3 | Effects of Y addition on NO and H_2O adsorption properties. In situ DRIFTS of NO desorption on (**a**) Pt/TiO_2 and (**b**) Pt/TiO_2 + Y catalysts, and (**c**) normalized peak intensity (at 1586 cm^{-1}) for NO adsorption on Pt/TiO_2 and Pt/TiO_2 + Y catalysts at different temperatures; (**d**) NO-TPD profiles, (**e**) in situ DRIFTS of H_2O adsorption at 120 °C, and (**f**) H_2O-TPD profiles on Pt/TiO_2 and Pt/TiO_2 + Y catalysts.

the NO adsorption onto Pt/TiO_2, concurrently fostering the desorption of NO from Pt/TiO_2 + Y. These findings were further supported by the NO-TPD results (Fig. 3d), revealing that the Pt/TiO_2 + Y system indeed exhibited notably reduced NO desorption intensity and lowered desorption temperature (242 °C) comparing to Pt/TiO_2 (278 °C).

Considering that H_2O is the primary product in the H_2-SCR reaction, the impact of Y addition on H_2O adsorption property was also investigated. The in situ DRIFTS of H_2O adsorption on both Pt/TiO_2 and Pt/TiO_2 + Y at 120 °C clearly showed distinct peaks at *ca.* 1630 cm^{-1}, indicative of adsorbed H_2O molecules[38]. Additionally, broad peaks at *ca.* 3200 cm^{-1} were observed, corresponding to the hydroxyl species derived from adsorbed H_2O with bending feature[38–40]. Comparing to the case on Pt/TiO_2, H_2O adsorption on Pt/TiO_2 + Y displayed more prominent peaks (Fig. 3e), suggesting the enhanced H_2O adsorption due to the presence of Y. This enhancement was also confirmed by the H_2O-TPD results (Fig. 3f), where more pronounced H_2O desorption peaks were observed on Pt/TiO_2 + Y. Other than the H_2O desorption peak observed at 223 °C on both catalysts, an additional desorption peak at 164 °C was detected only on Pt/TiO_2 + Y. This low-temperature peak could be attributed to the physically adsorbed H_2O on the Y zeolite.

To reveal the effect of H_2O adsorption on the H_2-SCR performance, the catalysts were either pre-dehydrated or pre-adsorbed with H_2O prior to the H_2-SCR testing. Under the testing condition without H_2O, Pt/TiO_2 + Y always outperformed Pt/TiO_2 in terms of NO_x conversion and N_2 selectivity (Fig. 4a, Supplementary Fig. 21a). Comparing to the situation with pre-dehydration, interestingly, the pre-adsorption of H_2O on both catalysts improved their H_2-SCR performance. This improvement was particularly significant regarding the NO_x conversion on Pt/TiO_2 catalyst, which exhibited relatively weaker H_2O adsorption capacity as confirmed earlier. The gas phase H_2O formation was monitored during the H_2-SCR reaction (Supplementary Fig. 21b). As expected, much faster increase in H_2O concentration was observed over both catalysts subjected to the pre-adsorption of H_2O comparing to those subjected to the pre-dehydration. It was noticeable that, as shown in Fig. 4b, a discernible correlation emerged between the elevation in NO_x conversion and the concurrent rise in gas phase H_2O concentration over Pt/TiO_2 catalyst. However, over Pt/TiO_2 + Y system, the rise in gas phase H_2O concentration exhibited a delay compared to the progression of NO_x conversion, suggesting the capture of in situ formed H_2O due to the presence of Y. To further confirm the promotion effect of in situ generated H_2O and to verify the effect of NO adsorption on the H_2-SCR activity, transient H_2-SCR testing was conducted at 100 °C (Fig. 4c). Using the NO_x concentrations when switching from Ar flow to H_2-SCR flow as baselines, significant decrease in NO_x concentrations was observed when switching from $H_2 + O_2$ flow to H_2-SCR flow, while obvious increase in NO_x concentrations was observed when switching from $NO + O_2$ flow to H_2-SCR flow, on both catalysts. Clearly, initiating a pre-flow of $H_2 + O_2$ yielded benefit on improving the H_2-SCR activity, while pre-flowing $NO + O_2$ inhibited the H_2-SCR reaction to a certain extent. Such inhibition caused by the $NO + O_2$ flow could be due to the extensive coverage of Pt sites by NO, impeding the activation of H_2[30]. At 100 °C, the complete oxidation of H_2 to H_2O could be achieved on both catalysts (Supplementary Fig. 18). Consequently, the benefit of pre-flowing $H_2 + O_2$ should be originated from the adsorption of in situ formed H_2O. The presence of H_2O could strongly inhibit the NO adsorption, as confirmed by the in situ DRIFTS (Fig. 4d) and NO-TPD (Fig. 4e) analyses conducted on Pt/TiO_2 catalyst. The physical mixing of Pt/TiO_2 with Y could further promote the adsorption of in situ generated H_2O (Fig. 3e, f), creating a H_2O-rich environment around the Pt sites and facilitating the formation of a H_2O-covered Pt surface. This surface could reduce the NO coverage on

https://doi.org/10.1038/s41467-024-52382-7

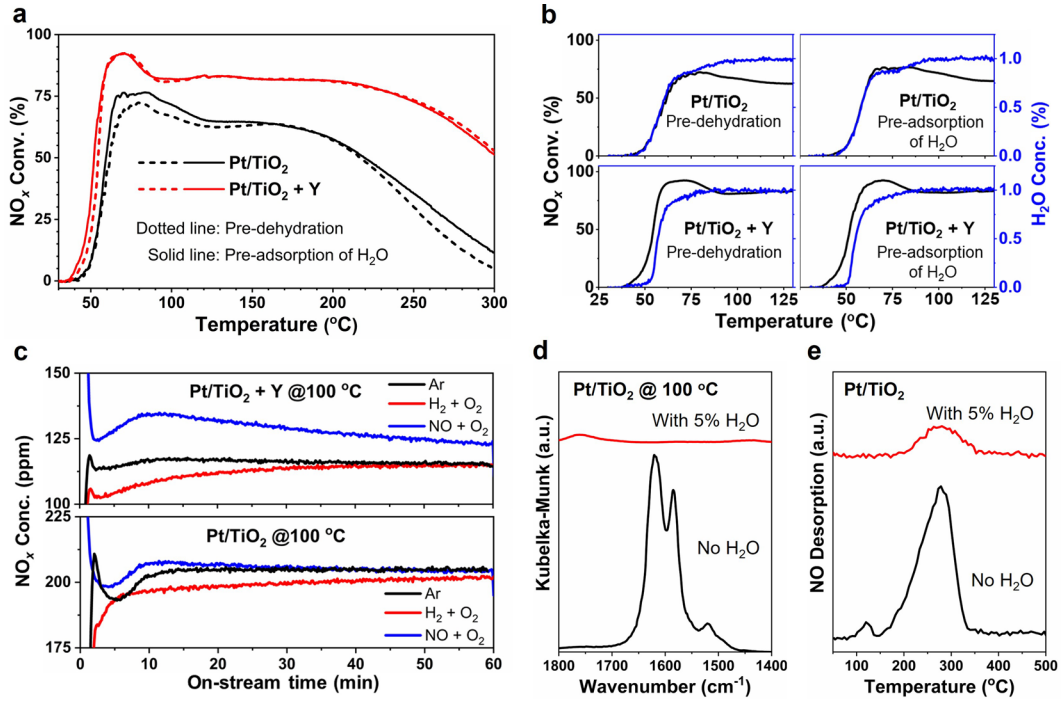

Fig. 4 | Effects of H_2O on the H_2-SCR performance and NO adsorption property. **a** NO_x conversion and (**b**) gas phase H_2O formation during the H_2-SCR reaction over Pt/TiO_2 and Pt/TiO_2 + Y catalysts with pre-dehydration at 300 °C or pre-adsorption of H_2O at 30 °C. Reaction conditions: 26 mg of Pt/TiO_2 catalyst, or a mixture containing 26 mg of Pt/TiO_2 and 26 mg of Y; transient-state light-off testing; 500 ppm NO, 1% H_2, and 10% O_2; WHSV = 461,540 mL·$g_{Pt/TiO2}^{-1}$·h^{-1}. **c** Time-resolved NO_x concentration after switching from different flows (Ar; or 1% H_2 + 10% O_2; or 500 ppm NO + 10% O_2) to H_2-SCR flow (500 ppm NO + 1% H_2 + 10% O_2) on Pt/TiO_2 and Pt/TiO_2 + Y catalysts at 100 °C. Testing conditions: 10 mg of Pt/TiO_2, or a mixture containing 10 mg of Pt/TiO_2 and 10 mg of Y; WHSV = 1,200,000 mL·$g_{Pt/TiO2}^{-1}$·h^{-1}. **d** In situ DRIFTS of NO adsorption at 100 °C, and (**e**) NO-TPD profiles on Pt/TiO_2 catalyst under the NO adsorption conditions with and without 5% H_2O.

Pt sites, thereby improving H_2 activation and H_2-SCR performance (Fig. 4a). However, introducing 5% external H_2O into the reaction flow could significantly inhibit the diffusion of NO and H_2 ($NO/H_2/H_2O$ molar ratio = 1/20/100) to the catalyst surface. Despite this inhibition resulting in the decreased activity for both catalysts, the Pt/TiO_2 + Y catalyst still exhibited significantly higher activity compared to the Pt/TiO_2 catalyst (Fig. 1a).

To elucidate the intrinsic promotion effect of Y addition to Pt/TiO_2 on the H_2-SCR performance, systematic density functional theory (DFT) calculations were performed. The Pt (111) surface was selected to represent the Pt active site in Pt/TiO_2 catalyst due to its high thermodynamic stability (Supplementary Fig. 22). As previously confirmed, the Y zeolite in Pt/TiO_2 + Y system possessed high ability to capture the in situ generated H_2O, creating the H_2O-rich environment around Pt sites. In light of this, a stable H_2O/Pt (111) interface was constructed (Supplementary Fig. 23), featuring a hydrogen bonding network with half of H_2O molecules dissociated on Pt with 2/3 monolayer (ML) coverage[41,42]. Such configuration was denoted as the H_2O/Pt (111) surface to represent the Pt active site in Pt/TiO_2 + Y system.

As shown in Supplementary Fig. 24, the Pt (111) surface was found more favorable for the NO adsorption with much higher free adsorption energy (−1.77 eV) comparing to that for H_2 adsorption (−0.87 eV) at the low coverage limit. Consequently, the optimal NO coverage on Pt (111) was firstly investigated by calculating the total Gibbs free adsorption energies, which was determined as 7/12 ML at relative low temperatures (T = 320-470 K and P_{NO} = 50 Pa) and in line with previous study[30]. With the highest total Gibbs free adsorption energy, the 7 NO/Pt (111) structure emerged as the most stable configuration (Fig. 5a, Supplementary Fig. 25), which was adopted as the starting point for studying the H_2 activation and reaction mechanism on Pt/TiO_2. On the stable H_2O/Pt (111) surface, the presence of a repulsive hydrogen bonding network led to a significant decline in the averaged free NO adsorption energies. Consequently, a notably reduced NO coverage (1/3 ML) was observed on the H_2O/Pt (111) surface (Fig. 5a, Supplementary Fig. 26), in comparison to the NO overage (7/12 ML) on the Pt (111) surface. Considering that the weakly-bonded *NO (T = 373 K, average G_{ads} = ~0.5 eV) was highly active and unstable, the H_2O/Pt (111) surface without *NO was used as the starting point for studying the H_2 activation and reaction mechanism on Pt/TiO_2 + Y. Accordingly, the H_2 adsorption and activation energies on 7 NO/Pt (111) and H_2O/Pt (111) surfaces were calculated, and the results are shown in Fig. 5b. Comparing to the endergonic process of H_2 adsorption (ΔG = 0.30 eV) and high H_2 activation barrier (G_a = 0.75 eV) observed on 7 NO/Pt (111) surface, an exergonic process of H_2 adsorption (ΔG = −0.63 eV) and much lower H_2 activation barrier (G_a = 0.30 eV) was found on H_2O/Pt (111) surface. Evidently, the H_2O/Pt (111) surface benefited the H_2 adsorption and activation, well aligned with the experimental results showing that Pt/TiO_2 + Y system exhibited superior H_2 activation ability comparing to Pt/TiO_2 (Supplementary Fig. 18).

The theoretical calculations of H_2-SCR reaction mechanism on Pt (111) and H_2O/Pt (111) surfaces were conducted to further elucidate the promotion effect of Y zeolite in Pt/TiO_2 + Y system. On Pt (111) surface, as shown in Supplementary Fig. 27 and Supplementary Table 5, the dissociation of *HNOH species into *NH and *OH was found to be the rate-determining step (RDS) for NO reduction with an activation energy (E_a) of 1.20 eV. Due to the high NO coverage, the inhibited H_2 activation further hindered the selective reduction of N-containing species to N_2, resulting in the high N_2O formation and low N_2 selectivity. In clear contrast, on H_2O/Pt (111) surface (Fig. 6, Supplementary Table 6), the *HNOH species could be readily dissociated into *NH and *OH with a lower activation energy of 0.24 eV (image viii to ix). Once the *NH species was formed, the gas phase NO could facilely couple with it to generate *HNNO, involving a substantial exothermicity of 2.31 eV (image ix to x). Interestingly, rather than releasing N_2O (with

https://doi.org/10.1038/s41467-024-52382-7

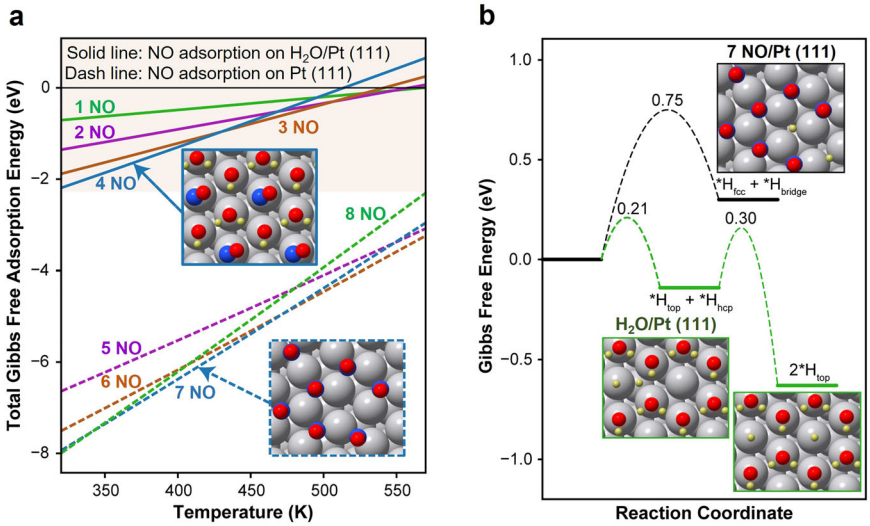

Fig. 5 | NO adsorption and H_2 activation on Pt (111) and H_2O/Pt (111) surfaces. **a** Total Gibbs free adsorption energy of NO molecules on Pt (111) and H_2O/Pt (111) surfaces. The reference state is the gas phase NO at 50 Pa. **b** Gibbs free energy diagram of H_2 activation on the 7 NO/Pt (111) surface and the H_2O/Pt (111) surface. The reference state is the gas phase H_2 at 1 atm. Color code: Pt (silver), O (red), N (blue), and H (yellow).

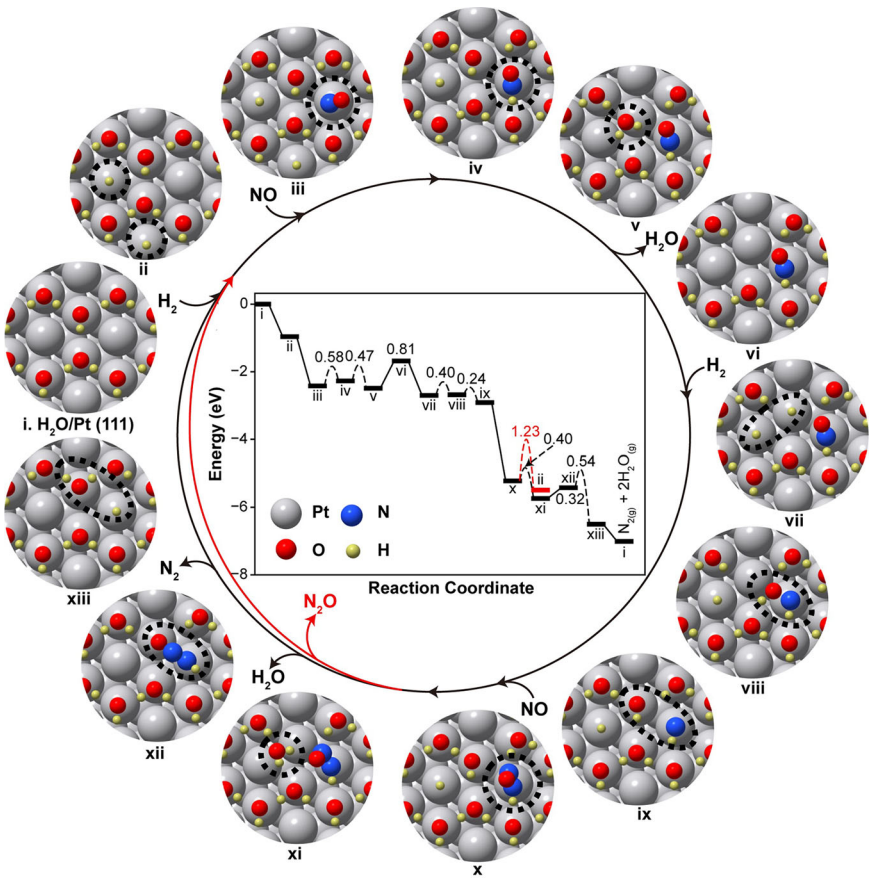

Fig. 6 | Potential energy diagrams and configurations for the H_2-SCR cycle on the Pt/TiO_2 + Y catalyst. The reaction was proposed to proceed on the H_2O/Pt (111) surface representing the structure of Pt/TiO_2 + Y catalyst under reaction conditions. The reaction energies and activation energies are indicated in eV in the diagram. Color code: Pt (silver), O (red), N (blue), and H (yellow). Corresponding energies are given in Supplementary Table 6.

E_a = 1.23 eV from image x to ii), the *HNNO species remained until an OH vacancy was facilely created in the hydrogen bonding network following the H_2O formation (E_a = 0.40 eV from image x to xi) and desorption (ΔE = 0.32 eV from image xi to xii). Subsequently, the *HNNO species was activated and dissociated, selectively producing N_2 with a barrier of 0.54 eV (image xii to xiii). Therefore, the RDS for NO reduction on H_2O/Pt (111) surface included both the creation of OH vacancy in the hydrogen bonding network and N_2 formation, with an overall activation energy of 0.86 eV (from image xi to xiii). Such activation energy for the RDS of H_2-SCR reaction on H_2O/Pt (111) surface was much lower than that on Pt (111) surface (1.20 eV). These simulation results well explained the significant promotion effect of Y zeolite

in Pt/TiO_2 + Y system for H_2-SCR in terms of both enhanced NO removal efficiency and elevated N_2 selectivity.

Discussion

A facile, universal and sustainable strategy of physically mixing Pt/oxide catalysts with zeolites has been successfully developed to improve the H_2-SCR performance of Pt-based catalysts for low-temperature NO_x removal. The Pt/TiO_2 + Y system exhibited superior H_2-SCR performance consistently in terms of NO_x conversion and N_2 selectivity, both before and after hydrothermal aging, as well as across various testing conditions. This catalyst system shows immense potential in H_2-SCR applications, particularly for H_2-ICE emission control. It was discovered that the incorporation of Y zeolite effectively promoted H_2O adsorption and the formation of H_2O-rich environment surrounding Pt active sites in Pt/TiO_2 + Y system. This consequently led to the reduction in excessive NO coverage and the improvement in H_2 activation, yielding substantial advantages for boosting both H_2-SCR efficiency and N_2 selectivity. In contrast to modifying the active sites through chemical methods, this study underscores the crucial importance of fine tuning the surrounding environment of active sites through an easy, sustainable physical mixing approach to achieve proficient heterogeneous catalysis.

Methods

Catalyst preparation

The Pt/oxide catalysts used in this study, including Pt/TiO_2, Pt/Al_2O_3, and Pt/SiO_2, were prepared using incipient wetness impregnation (IWI) method. A solution of colloidal Pt (2-6 nm) with 1 wt% Pt was added dropwise onto commercial anatase TiO_2 (surface area = 90 m^2/g), γ-Al_2O_3 (surface area = 150 m^2/g), or SiO_2 (surface area = 180 m^2/g) under stirring, followed by drying at 120 °C for 1 h. After calcination in air at 550 °C for 2 h with the temperature ramp of 5 °C/min, the catalysts were obtained and denoted as Pt/TiO_2, Pt/Al_2O_3, and Pt/SiO_2, respectively. As a reference, Pt/Y catalyst was also prepared by the same method using H-Y zeolite (SiO_2/Al_2O_3 molar ratio = 30) as support.

For physical mixing with Pt/oxide catalysts, commercial zeolites including H-Y (SiO_2/Al_2O_3 molar ratio = 30), H-ZSM-5 (SiO_2/Al_2O_3 molar ratio = 30), H-chabazite (CHA, SiO_2/Al_2O_3 molar ratio = 29), H-ferrierite (FER, SiO_2/Al_2O_3 molar ratio = 30), and H-Beta (SiO_2/Al_2O_3 molar ratio = 25) were used. TiO_2 or H-Y was also used to dilute Pt/TiO_2 or Pt/Y, respectively, for comparison. The content of additional zeolite/oxide was typically controlled at 50 wt% in the physically mixed samples, except for the Pt/TiO_2 + Y system with different Y contents of 33, 50, and 67 wt%. These mixed samples were denoted as Pt/oxide + zeolite or oxide. To simulate the catalyst throughout its operational lifespan in heavy-duty vehicles powered by diesel or hydrogen fuel, accelerated aging treatment under hydrothermal conditions of 550–650 °C for 50–100 h should be conducted. In this study, an aging treatment under 10% H_2O and 10% O_2 at 650 °C for 50 h was performed, and the resulting catalysts were labeled with "-Aged".

Catalyst characterizations

X-ray diffraction (XRD) measurement was performed on a PANalytical Empyrean diffractometer using a Cu Kα radiation source (λ = 0.15406 nm). The measurement covered the 5° to 80° range with a scan mode of 6 °/min and a scan step of 0.067°.

N_2 physisorption was used to determine the surface area, pore volume, and pore size distribution, which was performed on a Quantachrome Autosorb-iQ instrument at liquid nitrogen temperature (77 K). Prior to measurement, all samples were degassed at 300 °C for 2 h under vacuum. The N_2 adsorption-desorption isotherm was measured with 40 adsorption and 40 desorption points for Y and Pt/TiO_2 + Y samples, and with 20 adsorption and 20 desorption points for Pt/TiO_2 using the pressure intervals of $0 < P/P_0 < 1$. The surface area was calculated using the Brunauer–Emmett–Teller (BET) method based on the adsorption points in the relative pressure range between 0.05 and 0.3. The Horvath-Kawazoe (HK) method and non-local density functional theory (DFT) method were used to determine the pore volume and pore size distribution.

Transmission electron microscopy (TEM) and energy dispersive X-ray spectroscopy (EDS) mapping images were collected on a field emission FEI Tecnai F-30 with HAADF/ADF/BF STEM and EDS detectors operated at 200 kV.

The CO chemisorption measurement was performed on a Quantachrome Autosorb-iQ instrument. Before each measurement, the sample was first exposed to flowing He from room temperature to 150 °C at the ramp rate of 5 °C/min, and then held at 150 °C for 10 min. Next, the system was purged with 10% H_2/Ar, and the temperature was ramped to 400 °C at the rate of 5 °C/min and kept for 30 min. It is important to note that a certain degree of Pt sintering might occur during this reduction treatment, potentially resulting in a lower-estimated Pt dispersion value. The system was then switched back to He, while maintaining the temperature at 400 °C for 30 min. The final step involved cooling the system down to 35 °C in He at the rate of 20 °C/min, holding at 35 °C for 30 min, and injecting multiple CO pulses (5% CO/He) using thermal conductivity detector (TCD) to monitor the gas phase CO.

The X-ray absorption near-edge structure (XANES) and extended X-ray absorption fine structure (EXAFS) of Pt L_3-edge were measured at room temperature in fluorescent mode at beamline 7-BM QAS of the National Synchrotron Light Source II (NSLS-II), Brookhaven National Laboratory. Pt foil was measured during data collection for energy calibration and drift correction of the monochromator. Data analysis was conducted using Athena and Artemis from the Demeter software package. The processed EXAFS, $\chi(k)$, was weighted by k^2 to amplify the high-k oscillations. For Fourier-transformed (FT) spectra, the k range between 3.0 and 12.0 Å was used, and the curve fitting was performed using the Artemis software.

X-ray photoelectron spectroscopy (XPS) was measured on a Thermo Scientific ESCALAB 250Xi photoelectron spectrometer using Al K-α (hν = 1486.68 eV) as the X-ray source in ultrahigh vacuum condition (10^{-7} Pa). The binding energy (BE) of Pt 4*d* spectra was corrected using the C 1*s* signal at 284.6 eV as reference.

H_2 temperature-programmed reduction (H_2-TPR) was performed on the Quantachrome Autosorb-iQ instrument. Prior to testing, the samples were pretreated in a flow of 5% O_2/He at 300 °C for 1 h. After cooling down to 40 °C, a flow of 10% H_2/Ar was used, and the temperature was raised linearly from 40 to 700 °C at the ramp rate of 10 °C/min. The H_2 consumption was monitored on-line using TCD.

In situ DRIFTS experiments were performed on a Nicolet iS50 FTIR spectrometer equipped with a liquid nitrogen-cooled mercury-cadmium-telluride (MCT) detector and an in situ IR cell with ZnSe windows (DiffusIR, PIKE Technologies). Prior to measurements, all samples were pretreated in Ar flow at 300 °C for 1 h. The background spectra at different temperatures (e.g., 25, 100, 125, 150, 175, 200, 225, 250, 275, and 300 °C) were collected in Ar flow using 100 scans with a resolution of 4 cm^{-1}. For in situ DRIFTS of CO adsorption at 25 °C, 1% CO/Ar was introduced into the IR cell and kept for 30 min. Then, the samples were purged by Ar for 30 min to remove the weakly adsorbed CO, followed by spectra collection. For in situ DRIFTS of NO adsorption/desorption, the feed stream of 1000 ppm NO, 10% O_2, and 5% H_2O (when used) in Ar was introduced into the cell with a flow rate of 50 mL/min and kept for 60 min to achieve the saturated NO adsorption at 100 °C. The NO flow was then discontinued while Ar (50 mL/min) was kept flowing for 30 min to remove the gaseous and weakly adsorbed NO. Afterwards, the desorption experiments were carried out in Ar flow with the temperature elevated from 100 to 300 °C with an interval of 25 °C, and the spectra were collected under steady state accordingly. For in situ DRIFTS of H_2O adsorption, a feed stream of 5%

H_2O in Ar was introduced into the cell at a flow rate of 50 mL/min and kept for 60 min, achieving saturated H_2O adsorption at 120 °C. Then, the sample was purged with Ar for 30 min at 120 °C to remove the weakly adsorbed H_2O, and a background spectrum was collected. The sample was finally treated in Ar flow at 500 °C for 2 h and cooled down to 120 °C, followed by the spectrum collection.

NO temperature-programmed desorption (NO-TPD) and H_2O temperature-programmed desorption (H_2O-TPD) were conducted on a continuous flow fixed-bed system. A quartz tubular microreactor with an internal diameter of 4.0 mm was used, and a Hidden Analytical mass spectrometer (MS) was employed as detector. Typically, a feed stream of 1000 ppm NO, 10% O_2, and 5% H_2O (when used) in Ar was introduced into the reactor at a flow rate of 40 mL/min and kept for 60 min, achieving saturated NO adsorption at 50 °C. Afterwards, the sample was purged with Ar (40 mL/min) for 120 min at 50 °C to remove the weakly adsorbed molecules. The temperature was then elevated linearly from 50 to 600 °C at a ramp rate of 10 °C/min. For H_2O-TPD, a feed stream of 5% H_2O in Ar was introduced into the reactor at a flow rate of 40 mL/min and kept for 60 min, achieving saturated H_2O adsorption at 50 °C. The sample was then purged with Ar (40 mL/min) for 120 min at 50 °C to remove the weakly adsorbed H_2O. Subsequently, the temperature was elevated linearly from 50 to 600 °C at a ramp rate of 10 °C/min. The NO or H_2O desorption was monitored online using m/z of 30 or 18, respectively.

Catalytic performance evaluation

The catalytic activity evaluation for the H_2-SCR of NO_x over all catalysts was conducted using a continuous flow fixed-bed quartz tubular microreactor with an internal diameter of 4.0 mm. In each test, the catalyst or physical mixture containing 26 mg of Pt/oxide catalyst (40–60 mesh) was diluted with 0.25 g of inert SiC (40-60 mesh) to minimize the effect of hot spots. The reaction atmosphere comprised of 500 ppm NO, 1% H_2, 10% O_2, 5% CO_2 (when used) and 5% H_2O (when used), using Ar as balance. The total flow rate was controlled at 200 mL/min, resulting in a weight hourly space velocity (WHSV) of 461,540 $mL{\cdot}g_{Pt/oxide}^{-1}{\cdot}h^{-1}$. During the steady-state testing, the catalyst was held at each temperature for a duration of 30 min. Reactants and products were analyzed online by a MultiGas 2030 CEM-Cert FTIR spectrometer. The reactant conversion was defined as $(c_{inlet} - c_{outlet})/c_{inlet} \times 100\%$, where c_{inlet} and c_{outlet} were the inlet and outlet NO_x concentration in the feed stream, respectively. The N_2 selectivity was defined as $([NO]_{inlet} + [NO_2]_{inlet} - [NO]_{outlet} - [NO_2]_{outlet} - 2 \times [N_2O]_{outlet})/([NO]_{inlet} + [NO_2]_{inlet} - [NO]_{outlet} - [NO_2]_{outlet}) \times 100\%$. Under the H_2-SCR testing conditions with 1% H_2 and 10% O_2, NO could be either selectively reduced by H_2 to form N_2/N_2O or oxidized by O_2 to form NO_2. The NO selective conversion attributed to the NO reduction by H_2 ($NO + H_2$) under the H_2-SCR condition was defined as $([NO]_{inlet} + [NO_2]_{inlet} - [NO]_{outlet} - [NO_2]_{outlet})/([NO]_{inlet} - [NO]_{outlet}) \times 100\%$, and the NO conversion attributed to the NO oxidation by O_2 ($NO + O_2$) under the H_2-SCR condition was defined as $([NO_2]_{outlet} - [NO_2]_{inlet})/([NO]_{inlet} - [NO]_{outlet}) \times 100\%$. To avoid the significant heat or mass transfer limitation, the kinetics study was performed at 100 °C under the WHSV of 2,400,000 $mL{\cdot}g_{Pt/TiO2}^{-1}{\cdot}h^{-1}$ to determine the NO, H_2, and O_2 reaction orders on Pt/TiO_2 and Pt/TiO_2 + Y catalysts. The catalytic performance evaluations for separate NO oxidation, H_2-SCR in the presence of NO_2, H_2-SCR in the presence of NH_3, separate H_2 oxidation, as well as the H_2-SCR reaction on the catalysts with pre-dehydration and pre-adsorption of H_2O, were also conducted. The detailed information can be found in Supplementary Text 1.

DFT calculations

Periodic non-spin-polarized DFT calculations were performed using the Vienna Ab-initio Simulation Package (VASP) and the Perdew-Burke-Ernzerhof functional within generalized gradient approximation (GGA). The valence electrons were described by projector augmented wave pseudopotentials with an energy cutoff of 400 eV for all the calculations. The Methfessel-Paxton smearing scheme was used with a width of 0.15 eV and the precision was set to "accurate". The convergence criteria for energies and forces in structure optimizations were set as 10^{-5} eV and 0.02 eV $Å^{-1}$, respectively. The van der Waals (vdW) interactions were included via using Grimme's DFT-D3 method. The Brillouin zone for periodic slab calculations was sampled on Γ-centered Monkhorst-Pack type 2 × 3 × 1 k-point grid. Transition states of surface reactions were searched by the nudged elastic band (NEB) together with the dimer method. Further vibrational analysis was adopted to confirm the transition states. Only one imaginary frequency mode along the reaction trajectory represented the true saddle point.

The reaction energy (ΔE) of each elementary step was computed by the difference between the DFT energy of the final state (E_{FS}) and that of the corresponding initial state (E_{IS}), with $\Delta E = E_{FS} - E_{IS}$. Similarly, the activation energy was calculated using the equation, $E_a = E_{TS} - E_{IS}$, where E_{TS} was the DFT energy of corresponding transition state (TS). H binding energy (E_b(H)) was computed by the equation, $E_b(H) = E_{H/support} - E_{support} - 0.5E_{H2}$, where $E_{H/support}$, $E_{support}$ and E_{H2} were the DFT energies of support with the *H adsorbate, the support, and gas phase H_2, respectively. Gibbs free energy of each species was calculated by

$$G = E + E_{ZPE} + C_p T - TS \quad (1)$$

in which G was the Gibbs free energy, and E, E_{ZPE}, C_p and S were the DFT energy, zero point energy, heat capacity and entropy of each gas-phase species or surface intermediates, respectively. The E_{ZPE}, C_p, and S were calculated within the harmonic approximation. The Atomic Simulation Environment (ASE) package was employed to calculate the Gibbs free energy of gas and adsorbed species at certain temperatures and pressures.

The Gibbs free formation energies of adsorbates on corresponding surface were calculated via the following equation:

$$G_f(N_xO_yH_z/surface) = G(N_xO_yH_z/surface) - G(surface) - xG(NO) - (y - x) \times G(H_2O) - (z/2 - y + x) \times G(H_2) \quad (2)$$

in which $G(N_xO_yH_z/surface)$, G(surface), G(NO), $G(H_2O)$, and $G(H_2)$ were the Gibbs free energies of the surface with adsorbates, the clean surface, and gas phase NO, H_2O, and H_2 under relevant temperatures and pressures, respectively. The partial pressures of gas phase NO, H_2, and H_2O were set as 50, 1000, and 5000 Pa, which were within the range of experimental operation conditions.

Reporting summary

Further information on research design is available in the Nature Portfolio Reporting Summary linked to this article.

Data availability

Source data are provided with this paper.

References

1. Raza, S. A., Shah, N. & Sharif, A. Time frequency relationship between energy consumption, economic growth and environmental degradation in the United States: evidence from transportation sector. *Energy* **173**, 706–720 (2019).
2. Solaymani, S. CO_2 emissions patterns in 7 top carbon emitter economies: the case of transport sector. *Energy* **168**, 989–1001 (2019).
3. Stępień, Z. A comprehensive overview of hydrogen-fueled internal combustion engines: achievements and future challenges. *Energies* **14**, 6504 (2021).

4. Onorati, A. et al. The role of hydrogen for future internal combustion engines. *Int. J. Engine Res.* **23**, 529–540 (2022).
5. Luo, Q. H. et al. Experimental investigation of combustion characteristics and NO_x emission of a turbocharged hydrogen internal combustion engine. *Int. J. Hydrog.* **44**, 5573–5584 (2019).
6. Hu, Z. & Yang, R. T. 110th Anniversary: Recent progress and future challenges in selective catalytic reduction of NO by H_2 in the presence of O_2. *Int. J. Engine Res.* **58**, 10140–10153 (2019).
7. Liu, Z., Li, J. & Woo, S. I. Recent advances in the selective catalytic reduction of NO_x by hydrogen in the presence of oxygen. *Energy Environ. Sci.* **5**, 8799 (2012).
8. Borchers, M., Keller, K., Lott, P. & Deutschmann, O. Selective catalytic reduction of NO_x with H_2 for cleaning exhausts of hydrogen engines: Impact of H_2O, O_2, and NO/H_2 ratio. *Ind. Eng. Chem. Res.* **60**, 6613–6626 (2021).
9. Xie, S. et al. Silica modulated palladium catalyst with superior activity for the selective catalytic reduction of nitrogen oxides with hydrogen. *Appl. Catal. B Environ.* **327**, 122437 (2023).
10. Yang, S., Wang, X., Chu, W., Song, Z. & Zhao, S. An investigation of the surface intermediates of H_2-SCR of NO_x over Pt/H-FER. *Appl. Catal. B Environ.* **107**, 380–385 (2011).
11. Duan, K., Chen, B., Zhu, T. & Liu, Z. Mn promoted Pd/TiO_2–Al_2O_3 catalyst for the selective catalytic reduction of NO by H_2. *Appl. Catal. B Environ.* **176-177**, 618–626 (2015).
12. Park, D. C. et al. Widening the operating window of Pt/ZSM-5 catalysts for efficient NO_x removal in H_2-SCR: Insights from thermal aging. *Catal. Today* **425**, 114318 (2024).
13. Li, L., Wu, P., Yu, Q., Wu, G. & Guan, N. Low temperature H_2-SCR over platinum catalysts supported on Ti-containing MCM-41. *Appl. Catal. B Environ.* **94**, 254–262 (2010).
14. Zhang, X. et al. An investigation on N_2O formation route over Pt/HY in H_2-SCR. *Chem. Eng. J.* **252**, 288–297 (2014).
15. Dhainaut, F., Pietrzyk, S. & Granger, P. Kinetics of the NO+H_2 reaction over supported noble metal based catalysts: support effect on their adsorption properties. *Appl. Catal. B Environ.* **70**, 100–110 (2007).
16. Dhainaut, F., Pietrzyk, S. & Granger, P. Kinetics of the NO/H_2 reaction on $Pt/LaCoO_3$: a combined theoretical and experimental study. *J. Catal.* **258**, 296–305 (2008).
17. Machida, M., Ikeda, S., Kurogi, D. & Kijima, T. Low temperature catalytic NO_x–H_2 reactions over Pt/TiO_2-ZrO_2 in an excess oxygen. *Appl. Catal. B Environ.* **35**, 107–116 (2001).
18. Costa, C. N. & Efstathiou, A. M. Mechanistic aspects of the H_2-SCR of NO on a novel Pt/MgO-CeO_2 catalyst. *J. Phys. Chem. C* **111**, 3010–3020 (2007).
19. Costa, C. N. & Efstathiou, A. M. Low-temperature H_2-SCR of NO on a novel Pt/MgO-CeO_2 catalyst. *Appl. Catal. B Environ.* **72**, 240–252 (2007).
20. Park, S. M., Kim, M. Y., Kim, E. S., Han, H. S. & Seo, G. H_2-SCR of NO on Pt–MnO_x catalysts: reaction path via NH_3 formation. *Appl. Catal. A Gen.* **395**, 120–128 (2011).
21. Yu, Q. et al. The promotional effect of Cr on catalytic activity of Pt/ZSM-35 for H_2-SCR in excess oxygen. *Catal. Commun.* **11**, 955–959 (2010).
22. Komatsubara, M., Koga, A., Tanaka, M., Hagiwara, R. & Iwamoto, M. Three pathways to selective catalytic reduction of NO over Pt/Nb-AlMCM-41 under H_2 with excess O_2. *Catal. Sci. Technol.* **6**, 7398–7407 (2016).
23. Yu, Q. et al. Selective catalytic reduction of NO by hydrogen over Pt/ZSM-35. *Catal. Today* **158**, 452–458 (2010).
24. Zhang, X. et al. Promotion effect of tungsten on the activity of Pt/HZSM-5 for H_2-SCR. *Chem. Eng. J.* **260**, 419–426 (2015).
25. Wang, X., Wang, X., Yu, H. & Wang, X. The functions of Pt located at different positions of HZSM-5 in H_2-SCR. *Chem. Eng. J.* **355**, 470–477 (2019).
26. Burch, R. & Coleman, M. D. An investigation of promoter effects in the reduction of NO by H_2 under lean-burn conditions. *J. Catal.* **208**, 435–447 (2002).
27. Li, X., Zhang, X., Xu, Y., Liu, Y. & Wang, X. Influence of support properties on H_2 selective catalytic reduction activities and N_2 selectivities of Pt catalysts. *Chin. J. Catal.* **36**, 197–203 (2015).
28. Yazawa, Y. et al. The support effect on propane combustion over platinum catalyst: control of the oxidation-resistance of platinum by the acid strength of support materials. *Appl. Catal. A Gen.* **233**, 103–112 (2002).
29. Shibata, J. et al. Factors controlling activity and selectivity for SCR of NO by hydrogen over supported platinum catalysts. *J. Phys. Chem. B* **108**, 18327–18335 (2004).
30. Farberow, C. A., Dumesic, J. A. & Mavrikakis, M. Density functional theory calculations and analysis of reaction pathways for reduction of nitric oxide by hydrogen on Pt(111). *ACS Catal.* **4**, 3307–3319 (2014).
31. Liu, Z., Jia, B., Zhang, Y. & Haneda, M. Engineering the metal–support interaction on Pt/TiO_2 catalyst to boost the H_2-SCR of NO_x. *Ind. Eng. Chem. Res.* **59**, 13916–13922 (2020).
32. Kim, S. S. & Hong, S. C. Relationship between the surface characteristics of Pt catalyst and catalytic performance on the H_2-SCR. *J. Ind. Eng. Chem.* **16**, 992–996 (2010).
33. Sterlepper, S., Fischer, M., Claßen, J., Huth, V. & Pischinger, S. Concepts for hydrogen internal combustion engines and their implications on the exhaust gas aftertreatment system. *Energies* **14**, 8166 (2021).
34. Halasz, I. & Agarwal, M. Hydrophobic nano-layer on surface prevents H_2O adsorption in moderately aluminum deficient Y zeolite crystals. *Microporous Mesoporous Mater.* **310**, 110621 (2021).
35. Yao, X. et al. Selective catalytic reduction of NO_x by NH_3 over CeO_2 supported on TiO_2: comparison of anatase, brookite, and rutile. *Appl. Catal. B Environ.* **208**, 82–93 (2017).
36. Xie, S. et al. Copper single atom-triggered niobia–ceria catalyst for efficient low-temperature reduction of nitrogen oxides. *ACS Catal.* **12**, 2441–2453 (2022).
37. Meng, D. et al. A highly effective catalyst of Sm-MnO_x for the NH_3-SCR of NO_x at low temperature: promotional role of Sm and its catalytic performance. *ACS Catal.* **5**, 5973–5983 (2015).
38. Kipreos, M. D. & Foster, M. Water interactions on the surface of 50 nm rutile TiO_2 nanoparticles using in situ DRIFTS. *Surf. Sci.* **677**, 1–7 (2018).
39. Wu, J. et al. Breaking through water-splitting bottlenecks over carbon nitride with fluorination. *Nat. Commun.* **13**, 6999 (2022).
40. Rieth, A. J., Hunter, K. M., Dinca, M. & Paesani, F. Hydrogen bonding structure of confined water templated by a metal-organic framework with open metal sites. *Nat. Commun.* **10**, 4771 (2019).
41. Tripković, V., Skúlason, E., Siahrostami, S., Nørskov, J. K. & Rossmeisl, J. The oxygen reduction reaction mechanism on Pt(111) from density functional theory calculations. *Electrochim.Acta* **55**, 7975–7981 (2010).
42. Ogasawara, H. et al. Structure and bonding of water on Pt(111). *Phys. Rev. Lett.* **89**, 276102 (2002).

Acknowledgements

This work was supported by a research fund from BASF Environmental Catalyst and Metal Solutions and the Startup Fund (F.L.) from the University of California, Riverside (UCR). S.X., D.K. and X.Z. thank the support from the Preeminent Postdoctoral Program (P3) at the University of Central Florida (UCF). L.L. and H.X. thank the support from NSF CDS&E program (CBET-2245402). F.L. sincerely thanks Mr. Franck Thibaut and Ms. Corinne Lehaut from Tronox Inc., Dr. Marcos Schöneborn from Sasol, and Dr. Chris Bauer from Evonik for providing raw materials in catalyst synthesis. F.L. and S.X. thank Dr. Tangyuan Li and Prof. Liangbing Hu from the University of Maryland for their assistance with N_2

physisorption testing. This research used beamline 7-BM (QAS) of the National Synchrotron Light Source II, a U.S. Department of Energy (DOE) Office of Science User Facility operated for the DOE Office of Science by Brookhaven National Laboratory under Contract No. DE-SC0012704. H.X. acknowledges the computational resource provided by the advanced research computing at Virginia Polytechnic Institute and State University.

Author contributions

F.L. and Y.L. conceived the idea and directed the project. S.X. designed the experiments, performed the experiments, and analyzed the data. K.Y., D.K. and X.Z. assisted with the catalyst testing and characterization. L.M. and S.E. conducted XAS measurements. L.L. and H.X. performed DFT calculations and analysis. S.X. and L.L. wrote the manuscript. F.L. and H.X. mentored the manuscript writing and revision. All authors discussed the results and commented on the manuscript.

Competing interests

The authors declare no competing interests.

Additional information

Supplementary information The online version contains supplementary material available at https://doi.org/10.1038/s41467-024-52382-7.

Correspondence and requests for materials should be addressed to Hongliang Xin or Fudong Liu.

Peer review information *Nature Communications* thanks Unai De-La-Torre and the other, anonymous, reviewers for their contribution to the peer review of this work. A peer review file is available.